International Journal of Applied Electromagnetics and Mechanics 21 (2005) 51–62
IOS Press

Image and conductivity reconstruction of a variable conducting cylinder in a half-space

Wei Chien, Chien-Ching Chiu* and Ching-Lieh Li
Electrical Engineering Department, Tamkang University, Tamsui, Taiwan

Abstract. In this paper we address an inverse scattering problem whose aim is to determine the geometrical and the physical properties of a variable conducting cylindrical body buried in a half-space. The variable conductivity boundary leads to a mathematically ill-posed nonlinear equation. To overcome this difficulty, the attained system of nonlinear integral equations is reformulated into an optimization problem and solved by using the genetic algorithm. The genetic algorithm is employed to search the global extreme of the object function, such that the shape and the variable conductivity of the scatterer can be reconstructed. Even when the initial guess is far away from the exact one, the genetic algorithm can avoid the local extreme and attain to a global extreme solution sucessfully. In such a case, the gradient-based methods often get stuck in a local extreme. It is found that multiple incident waves from different directions permit good reconstruction of the shape and, to a lesser extent, the conductivity in the presence of noise for the measured data. Numerical results are given to show the effectiveness of the genetic algorithm.

1. Introduction

Due to the large area of applications such as non-destructive problems, geophysical prospecting and determination of underground tunnels and pipelines, etc, the inverse scattering problems related to the buried bodies are of particular importance in the scattering theory. In the past 20 years, many rigorous methods have been developed to solve the exact equations [1–9]. However, inverse problems of this type are difficult to solve because they are ill-posed and nonlinear [10]. As a result, many inverse problems are reformulated into optimization ones and then numerically solved by different iterative methods such as the Newton-Kantorovitch method [1–5], the Levenberg-Marquardt algorithm [6–8], and the successive-overrelaxation method [9]. Most of these approaches employ the gradient-based searching scheme to find the extreme of the cost function, which are highly dependent on the initial guess and usually get trapped in the local extreme. The genetic algorithm [11] is an evolutionary algorithm that uses the stochastic mechanism to search through the parameter space. As compared to the gradient-based searching techniques, the genetic algorithm is less prone to converge to a local extreme. This renders it an ideal candidate for global optimization. A few papers had applied the genetic algorithm to reconstruct the shape of a conductor [12–16]. However, to the best of our knowledge, there are still no numerical results by using the genetic algorithm for the buried variable conducting scatterers. In this paper, we present a computational method to recover the shape of a buried variable conducting cylinder based on the genetic algorithm. In Section 2, the theoretical formulation for the inverse scattering is reported. The general principle of the genetic algorithms and the way we apply them are described. Numerical results are given for various objects of different shapes in Section 3. Finally, some conclusions are drawn in Section 4.

*Corresponding author. E-mail: chiu@ee.tku.edu.tw.

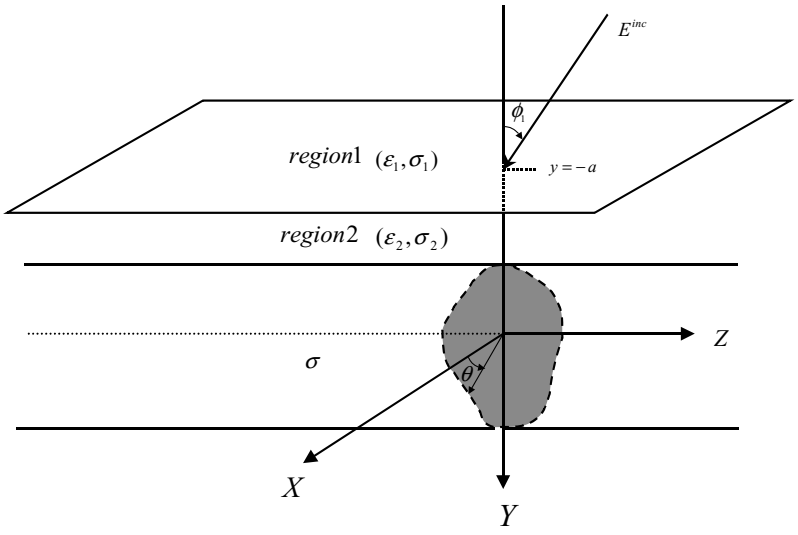

Fig. 1. Geometry of the proposed problem in (x, y) plane.

2. Theoretical formulation

Let's consider a variable conducting cylinder with finite conductivity profile buried in a lossy homogeneous half-space, as shown in Fig. 1. The media in regions 1 and 2 are characterized by the permittivity and conductivity $(\varepsilon_1, \sigma_1)$ and $(\varepsilon_2, \sigma_2)$, respectively, while the permeability μ_0 is used for each region, i.e., only non-magnetic media are concerned here. The cross section of the cylinder is described by polar coordinates in the xy plane through the shape function $\rho = F(\theta)$. The cylinder is illuminated by a plane wave with time dependence exp $(j\omega t)$, of which the electric field is assumed parallel to the z-axis (i.e., transverse magnetic or TM polarization). Let E^{inc} denote the incident E field from region 1 to region 2 with incident angle ϕ_1. Owing to the interface between region 1 and region 2, the incident plane wave would generate two waves in the absence of the conducting object: the reflected wave (for $y \leqslant -a$) and the transmitted wave (for $y > -a$). Thus the unperturbed field is given by

$$\vec{E}_i(\vec{r}) = E_i(x, y)\hat{z} \tag{1}$$

with

$$E_i(x,y) = \begin{cases} E_1(x,y) = e^{-jk_1[x\sin\phi_1+(y+a)\cos\phi_1]} + R_1 e^{-jk_1[x\sin\phi_1-(y+a)\cos\phi_1]}, & y \leqslant -a \\ E_2(x,y) = Te^{-jk_2[x\sin\phi_2+(y+a)\cos\phi_2]} & y > -a \end{cases}$$

where

$$R_1 = \frac{1-n}{1+n}, T = \frac{2}{1+n}, n = \frac{\cos\phi_2}{\cos\phi_1}\sqrt{\frac{\varepsilon_2 - j\sigma_2/\omega}{\varepsilon_1 - j\sigma_1/\omega}}$$

$$k_1 \sin\phi_1 = k_2 \sin\phi_2$$

$$k_i^2 = \omega^2\varepsilon_i\mu_0 - j\omega\mu_0\sigma_i, i = 1, 2 \text{ with } \mathrm{Im}\,(k_i) \leqslant 0$$

As the buried object is present, the scattered field can be expressed by

$$E_s(x,y) = -\int_0^{2\pi} G(x,y;F(\theta'),\theta')J(\theta')d\theta' \tag{2}$$

with

$$J(\theta) = -j\omega\mu_0\sqrt{F^2(\theta)+F'^2(\theta)}J_s(\theta)$$

$$G(x,y;x',y') = \begin{cases} G_1(x,y;x',y'), & y \leqslant -a \\ G_2(x,y;x',y') = G_f(x,y;x',y') + G_s(x,y;x',y'), & y > -a \end{cases} \tag{3}$$

where

$$G_1(x,y;x',y') = \frac{1}{2\pi}\int_{-\infty}^{\infty} \frac{j}{\gamma_1+\gamma_2} e^{j\gamma_1(y+a)} e^{-j\gamma_2(y'+a)} e^{-j\alpha(x-x')} d\alpha \tag{3a}$$

$$G_f(x,y;x',y') = \frac{j}{4} H_0^{(2)}[k_2\sqrt{(x-x')^2+(y-y')^2}] \tag{3b}$$

$$G_s(x,y;x',y') = \frac{1}{2\pi}\int_{-\infty}^{\infty} \frac{j}{2\gamma_2}\left(\frac{\gamma_2-\gamma_1}{\gamma_2+\gamma_1}\right) e^{-j\gamma_2(y+2a+y')} e^{-j\alpha(x-x')} d\alpha \tag{3c}$$

$$\gamma_i^2 = k_i^2 - \alpha^2, i = 1,2,\ \mathrm{Im}\,(\gamma_i) \leqslant 0, y' > a$$

Here $J_s(\theta)$ is the induced surface current density that is proportional to the normal derivative of the electric field on the conductor surface. $G(x,y;x',y')$ is the Green's function in terms of the Fourier transform [3]. Note that we might face some difficulties in calculating the Green's function since the Green's function, given by Eq. (3), take the form of an improper integral that must be evaluated numerically. However, the integral converges very slowly when (x,y) and (x',y') approach the interface, for which the acceleration of converging speed is possible by rewriting the Green's function as a closed-form term plus a rapidly converging integral (see appendix). In Eq. (3b), $H_0^{(2)}$ is the Hankel function of the second kind of order zero. For a variable conducting scatterer with finite conductivity, the electromagnetic wave is able to penetrate into the interior of the scatterer such that the total tangential electric field at the surface of the scatterer is not equal to zero. As described in [17] and [18], the boundary condition for this case can be approximated by assuming that the total tangential electric field on the scatterer surface is related to surface current density through a surface impedance $Z_s(\omega,\theta)$:

$$\hat{n}\times\vec{E} = \hat{n}\times(Z_s\vec{J}_s) \tag{4}$$

where $\hat{n}$ is the outward unit vector normal to the surface of the scatterer. Assuming the scatterer of interest here is a nonmagnetic and imperfectly conducting cylinder with minimum radius of curvature denoted by a. The surface impedance can be expressed by $Z_s(\omega,\theta) \cong \sqrt{j\omega\mu_0/\sigma\,(\theta)}$ as given in [17] and [18]. This approximation is valid as long as $|Im(N_c)ka| >> 1$ and $\sigma\,(\theta) \gg \omega\varepsilon_0$, where "Im" means taking the imaginary part, and N_c is the complex index of refraction of the conductor, given by

$N_c = \sqrt{1 + \frac{\sigma(\theta)}{j\omega\varepsilon_0}}$. The boundary condition at the surface of the scatterer given by Eq. (4) then leads to an integral equation for $J(\theta)$:

$$E_2\left(F\left(\theta\right),\theta\right) = \int_0^{2\pi} G_2\left(F\left(\theta\right),\theta;F\left(\theta'\right),\theta'\right) J\left(\theta'\right) d\theta' + j\sqrt{\frac{j}{\omega\mu_0\sigma\left(\theta\right)}}\frac{J\left(\theta\right)}{\sqrt{F^2\left(\theta\right)+F'^2\left(\theta\right)}} \quad (5)$$

The total field E^{out} in region 1 is given by

$$E^{out}(r) = E_1(r) - \int_0^{2\pi} G_1(r;F(\theta'),\theta')J(\theta')d\theta' \quad (y \leqslant -a) \quad (6)$$

The direct problem is to compute the total field in region 1 when the shape function $F(\theta)$ is given. This can be achieved by first solving for J from Eq. (5) and then calculating E^{out} by Eq. (6).

For numerical calculation of the direct problem, the contour is first divided into sufficient small segments so that the induced surface current can be considered constant over each segment. Then the moment method is employed to solve Eqs (5) and (6) with pulse basis functions for expanding and the Dirac delta functions for testing [19].

For the inverse problem, the scattered electric fields E_s measured outside the scatterer, are used to determine the shape $F(\theta)$ and the conductivity of the object. Assume the approximate center of the scatterer, which in fact can be any point inside the scatterer, is known. Then the shape function $F(\theta)$ can be expanded as:

$$F\left(\theta\right) \cong \sum_{n=0}^{\frac{N}{2}} B_n \cos\left(n\theta\right) + \sum_{n=1}^{\frac{N}{2}} C_n \sin\left(n\theta\right) \quad (7)$$

$$\sigma(\theta) = \sum_{m=0}^{M/2} D_m \cos(m\theta) + \sum_{m=1}^{M/2} E_m \sin(m\theta) \quad (8)$$

where B_n, C_n, D_m and E_m are the real coefficients to be determined, and $(N+1)+(M+1)$ is the number of the unknowns. Note that the discretization number of $J(\theta)$ for the inverse problem must be different from that for the direct problem. Since it is crucial that the synthetic data generated by a direct solver are not like those obtained by the inverse solver, the discretization number for the direct problem is twice of that for the inverse problem in this study. For the inversion procedure, the genetic algorithm is employed to maximize the following object function:

$$SF = \left\{\frac{1}{X_T}\sum_{i=1}^{X_T}\left|E_s^{\exp}\left(\vec{r}_i\right) - E_s^{cal}\left(\vec{r}_i\right)\right|^2 \Big/ \sum_{i=1}^{X_T}\left[\left|E_s^{\exp}\left(\vec{r}_i\right)\right|^2 + \beta\left|F'\left(\theta\right)\right|^2\right]\right\}^{-1/2} \quad (9)$$

where X_T is the total number of measurement points, and $E_s^{cal}(\vec{r})$ and $E_s^{\exp}(\vec{r})$ are the calculated scattered field and the measured scattered field, respectively. Note that there is a regularization term $\beta\left|F'\left(\theta\right)\right|^2$ added in Eq. (9). The added term $\beta\left|F'\left(\theta\right)\right|^2$ can, to a certain extent, be interpreted as the smoothness requirement for the shape function $F(\theta)$. Therefore, the maximization of SF can be interpreted as the minimization of the least-square error between the measured and the calculated fields with the constraint

of smooth boundary. Typical values of β range from 0.00001 to 10. The optimal value of β depends mostly on the dimensions of the geometry. One can always choose a large enough value to ensure the convergence, although overestimation would result in a very smooth reconstructed image. Technically, we can let the value of β decrease gradually during the course of convergence [6].

Genetic algorithms are the global optimization methods based on the genetic recombination and evoluation in nature [11]. They use the iterative optimization procedures that start with a randomly generated population of potential solutions, and then gradually evolve toward a better solution through the application of the genetic operators. Genetic algorithms typically operate on a discretized and coded representation of the parameters rather than on the parameters themselves. These representations are considered as the "chromosomes", while the elements that constitutes the chromosome are called "genes". Simple but often very effective chromosome representations for optimization problem involving several continuous parameters can be obtained through the juxtaposition of discretized binary representations of the individual parameters. In our problem the parameters B_n, C_n, D_m and E_m are given by the following equation. As an example B_n is shown

$$B_n = p_{\min} + \frac{p_{\max} - p_{\min}}{2^L - 1} \sum_{i=0}^{L-1} b_i^{B_n} 2^i \tag{10}$$

where $b_0^{B_n}$, $b_1^{B_n}, \ldots$ and $b_{L-1}^{B_n}$ (gene) are the L-bit string of the binary representation of B_n, and $p_{\min}$ and $p_{\max}$ are the minimum and the maximum values admissible for B_n. Similar expressions exist for the parameters C_n, D_m and E_m and are omitted here for brevity. Here, $p_{\min}$ and $p_{\max}$ can be determined by prior knowledge of the object. Also, the finite resolution with B_n (C_n, D_m or E_m) can be tuned in practice by changing the number of bits assigned to it. The unknown coefficients in Eqs (7), (8) and (10) would then be described by a string (chromosome) with $(N + M + 2) \times L$ bits in total. The flow chart of a basic GA is shown in Fig. 2, which starts with a large initial population containing a total of X random chromosomes. Then, the GA iteratively generates a new population that offspring from the previous population through the application of the reproduction, crossover, and mutation operators.

The new population contain increasingly better chromosomes and will eventually converge to a population that consists of the optimal chromosomes. As soon as the cost function (CF) changes by $<$ 1% in two successive generations or exceeds 1000 generations, the genetic algorithm will be terminated and the final solution is then obtained.

3. Numerical results

Let us consider a variable conducting cylinder buried in a lossless half-space ($\sigma_1 = \sigma_2 = 0$). The permittivities in region 1 and region 2 are characterized by $\varepsilon_1 = \varepsilon_0$ and $\varepsilon_2 = 2.56\varepsilon_0$, respectively. A TM polarization plane wave of unit amplitude is incident from region 1 upon the object in region 2 as shown in Fig. 1. The frequency of the incident wave is chosen to be 3 GHz, of which the wavelength λ_0 in free space is 0.1 m. The object is buried at a depth $a \cong \lambda_0$ and the scattered fields are measured on a probing line along the interface between region 1 and region 2. The goal is to reconstruct the shape and the variable conductivity of the object by using the measured scattered field due to multiple incident waves from different angles. The object is illuminated by three incident waves from different directions, while 20 measurement points at equal spacing are used along the interface $y = -a$ for each incident angle. There are 60 measurement points in each simulation. The measurement is taken from $x = 0$ to

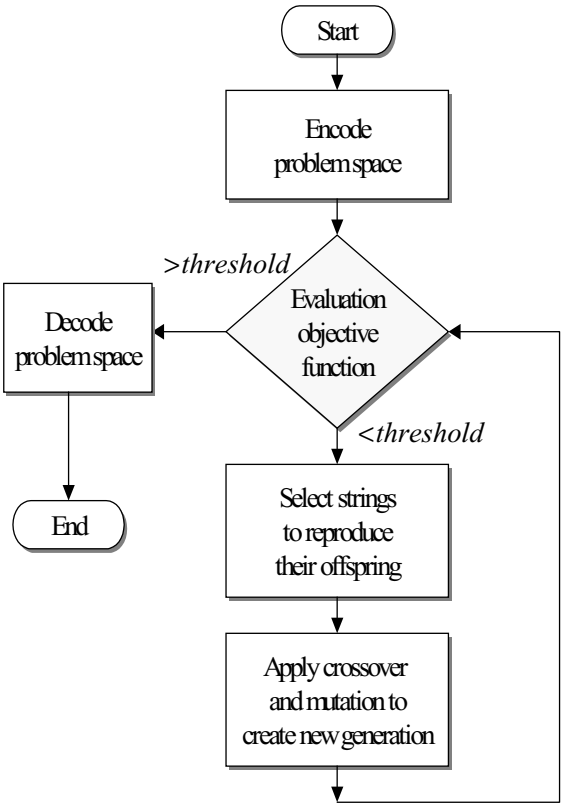

Fig. 2. Flow chart for the genetic algorithm.

0.2 m for incident angle $\phi_1 = -60°$, from $x = -$ 0.1 to 0.1 m for incident angle $\phi_1 = 0°$, and from $x = -$ 0.2 to 0m for incident angle $\phi_1 = 60°$. To save computing time, the number of unknowns is set to 16 (i.e. $N + M + 2 = 14$), and the population size is chosen as 300 (i.e. $X = 300$). The binary string length of the unknown coefficients B_n, C_n, D_m and E_m is set to 16 (i.e., $L = 16$). In other words, the bit number of a chromosome is 224. The search ranges for the unknown coefficients of the shape function are chosen to be from 0 to 0.1 and the unknown coefficients of the conductivity function are chosen to be from 1 to 100. The extreme values of the coefficients of the shape function and conductivity function can be determined by some priori knowledge of the objects. Here, the prior knowledge means that we can get the approximate position and the size of the buried cylinder by first using tomography technique, and then get the exact solution by the genetic algorithm. The crossover probability p_c and mutation probability p_m are set to be 0.8 and 0.1, respectively. The value of β in Eq. (9) is chosen to be 0.001.

In the first example, the shape function is given by $F(\theta) = (0.03+0.012\cos 2\theta)$ m and the conductivity function by $\sigma(\theta) = (80 + 15\cos\theta + 15\sin 2\theta)$ S/m. The reconstructed shape function and conductivity function for the best population member (chromosome) are plotted in Fig. 3(a) and (b), respectively. The errors for the reconstructed shape DR and the reconstructed conductivity DSIG are shown in Fig. 3(c), of which DR and DSIG are defined as

$$DR = \left\{ \frac{1}{N'} \sum_{i=1}^{N'} [F^{cal}(\theta_i) - F(\theta_i)]^2 / F^2(\theta_i) \right\}^{1/2} \tag{11}$$

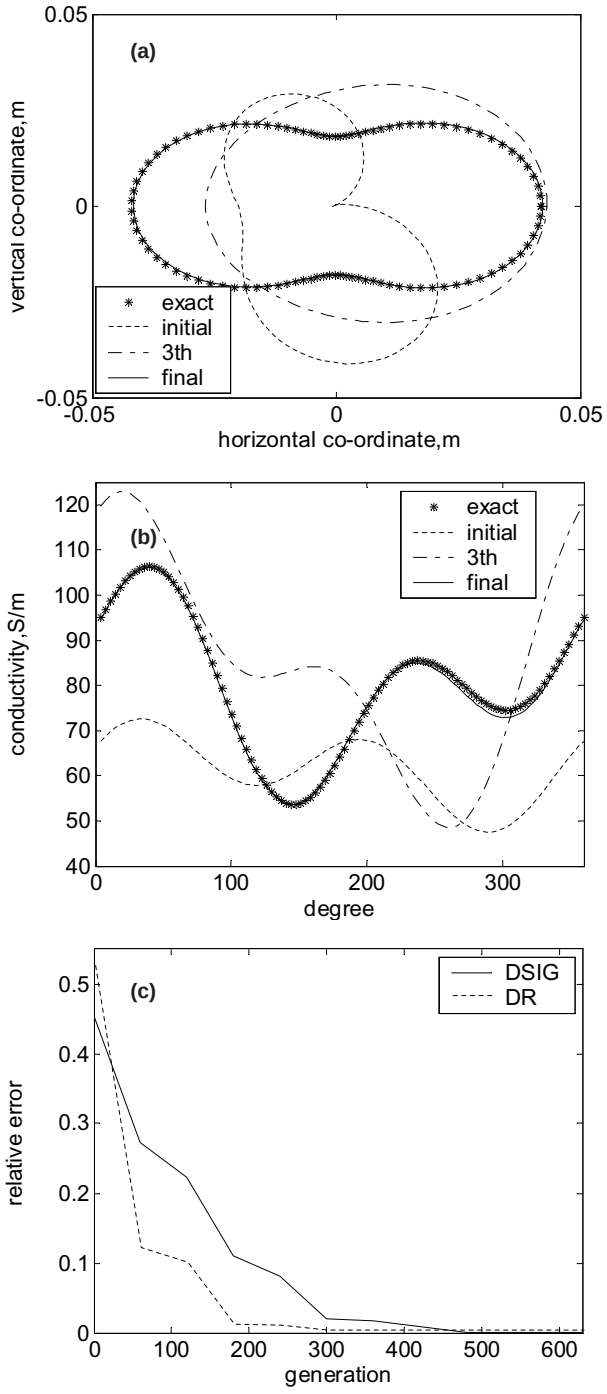

Fig. 3. (a) Shape function for example 1. The star curve represents the exact shape, while the other curves are the calculated shapes in iterative process. (b) Conductivity function for example 1. The star curve represents the exact conductivity, while the other curves are the calculated conductivities in iterative process. (c) The shape and conductivity function errors versus generation.

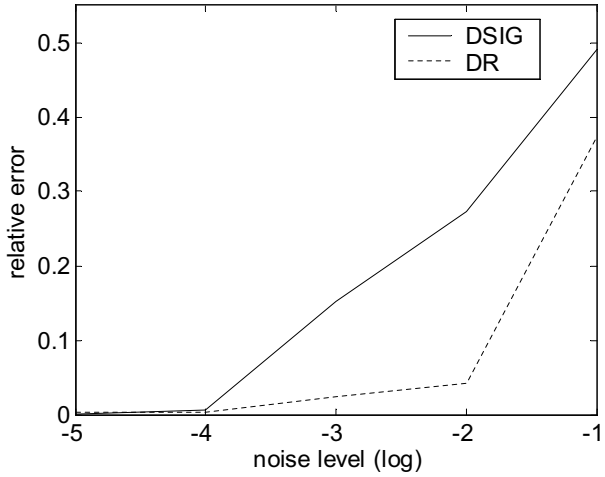

Fig. 4. The relative errors of shape and conductivity as functions of the noise.

$$DSIG = \left\{ \frac{1}{N'} \sum_{i=1}^{N'} [\sigma^{cal}(\theta_i) - \sigma(\theta_i)]^2 / \sigma^2(\theta_i) \right\}^{1/2} \tag{12}$$

where N' is set to 60. The quantities DR and DSIG provide measures of how well $F^{cal}(\theta)$ approximates$F(\theta)$ and $\sigma^{cal}(\theta)$ approximates $\sigma(\theta)$, respectively. From Fig. 3(a) and (b), it is clear that the reconstruction of the shape function and conductivity function is quite good. Note that the initial guess is far away from the exact one. In such a case, the gradient-based methods often get stuck in a local extreme and can't find the exact shape and conductivity of the scatterer. In addition, it is observed that the reconstruction of conductivity function converges toward the exact value only after DR is small enough. This is consistent with the fact that the shape function contributes more to the scattered E field than the conductivity function does. In other words, the reconstruction of the shape function has a higher priority than the reconstruction of the conductivity function. For the simulation, the needed CPU time is about 2 hours for this case on a Celeron 2.0 GHz Computer. To investigate the sensitivity of the imaging algorithm against random noise, two independent Gaussian noises with zero mean have been added to the real and imaginary parts of the simulated scattered fields. Normalized standard deviations of 10^{-5}, 10^{-4}, 10^{-3}, 10^{-2} and 10^{-1} are used in the simulations. The normalized standard deviation mentioned earlier is defined as the standard deviation of the Gaussian noise divided by the rms value of the scattered E fields. Here, the signal-to-noise ratio (SNR) is inversely proportional to the normalized standard deviation. The reconstructed errors vs noise level for this example are plotted in Fig. 4. It is found that the effect of noise is negligible for normalized standard deviations below 10^{-3}. It is also observed that the reconstructed conductivity is more sensitive to the noise than the reconstructed shape is.

In the second example, we select the following shape function $F(\theta) = (0.03 + 0.005\cos\theta - 0.005\cos 2\theta + 0.005\cos 3\theta)$ m and conductivity function $\sigma(\theta) = (80 + 15\cos 2\theta + 15\sin\theta + 20\sin 3\theta)$ S/m. The purpose of this example is to show the capability of the proposed method to reconstruct a scatter whose shape and conductivity function has two concavities. Satisfactory results are shown in Fig. 5(a) and 5(b).

In the third example, the shape and conductivity function are selected to be $F(\theta) = (0.05 + 0.01\sin\theta + 0.01\sin 2\theta + 0.01\sin 3\theta)$ m and $\sigma(\theta) = (80 + 12\cos\theta + 12\sin 2\theta + 24\sin 3\theta)$ S/m, respectively. Note

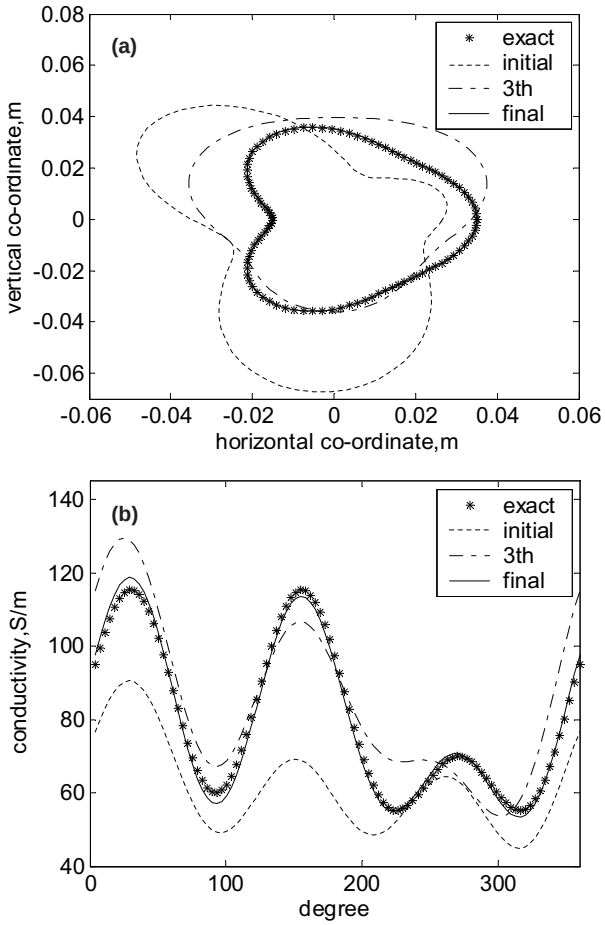

Fig. 5. (a) Shape function for example 2. The star curve represents the exact shape, while the other curves are the calculated shapes in iterative process. (b) Conductivity function for example 2. The star curve represents the exact conductivity, while the other curves are the calculated conductivities in iterative process.

that the shape function is not symmetrical about either x axis or y axis. This example is to further verify the reliability of the algorithm. Refer to Fig. 6(a) and 6(b) for details. It is concluded that satisfactory results can be obtained as long as the noise level is $< 10^{-3}$.

4. Conclusions

We have presented a study of applying the genetic algorithm to reconstruct the shape and conductivity of a buried metallic object through the measured of scattered E fields. Based on the boundary condition and the measured scattered fields, we have derived a set of nonlinear integral equations and reformulated the imaging problem into an optimization one. By using the genetic algorithm, the shape and conductivity of the object can be reconstructed, even when the initial guess is far from exact one. The genetic algorithm converges to a global extreme of the cost function, while the gradient-based methods often get stuck in a local extreme. Good reconstruction has been achieved from the measured scattered fields both with and without the additive Gaussian noise. Numerical results also illustrate that the conductivity

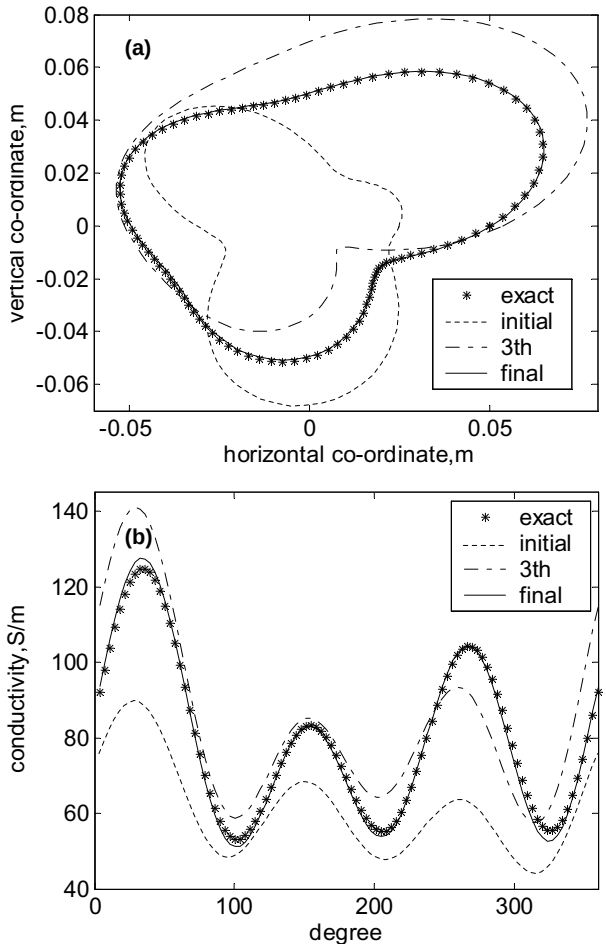

Fig. 6. (a) Shape function for example 3. The star curve represents the exact shape, while the other curves are the calculated shapes in iterative process. (b) Conductivity function for example 3. The star curve represents the exact conductivity, while the other curves are the calculated conductivities in iterative process.

reconstruction is more sensitive to noise than the shape recontruction is. According to our experience, the main difficulties in applying the genetic algorithm to this problem lie on the choice of the parameters, such as the population size (X), bit length of the string (L), crossover probability (p_c), and mutation probability (p_m). Different parameter sets will affect the speed of convergence as well as the computation time required. From the numerical simulation, it is found that the population size from 300 to 600, the string length from 8 to 16 bits, p_c and p_m in the ranges of $0.7 < p_c < 0.9$ and $0.0005 < p_m < 0.05$ are suitable for the imaging problems of this type.

Acknowledgment

This work was supported by National Science Council, Republic of China, under Grant NSC-90-2213-E-032-022.

Appendix

To calculate the Green's function, we can use the following formula.

$$\int_u^\infty x^{r-1}e^{-\beta x}\cos\delta x dx = \frac{1}{2}(\beta+j\alpha)^{-r}\Gamma\left[r,(\beta+j\delta)u\right] + \frac{1}{2}(\beta-j\alpha)^{-r}\Gamma\left[r,(\beta-j\delta)u\right] \quad \text{for } \mathrm{Re}\,\beta > |\mathrm{Im}\delta| \tag{A1}$$

where $\Gamma(\alpha,Z)=\int_z^\infty e^{-t}t^{\alpha-1}dt$

Γ is the incomplete Gamma function that satisfies

$$\Gamma(-n,z) = \frac{(-1)^n}{n!}\left[\Gamma(0,Z) - e^{-z}\sum_{m=0}^{n-1}(-1)^m\frac{m!}{z^{m+1}}\right]$$
$$\Gamma(0,z) = -\gamma - \ln z - \sum_{n=1}^{\infty}(-1)^n\frac{z^n}{(n+1)!}\left[|\arg(z)|<\pi\right] \tag{A2}$$

in which γ is Euler's constant, i.e., $\gamma = 0.5772156649$.

Let us consider the following integral

$$G_1 = \frac{1}{2\pi}\int_{-\infty}^{\infty}\frac{j}{\gamma_1+\gamma_2}e^{j\gamma_1(y+a)}e^{-j\gamma_2(y'+a)}e^{-j\alpha(x-x')}d\alpha$$
$$= \frac{1}{\pi}\int_0^{\infty}\frac{j}{\gamma_1+\gamma_2}e^{j\gamma_1(y+a)}e^{-j\gamma_2(y'+a)}\cos\alpha(x-x')d\alpha$$

where $\gamma_i^2 = k_i^2-\alpha^2, i=1,2,3$ $\mathrm{Im}(\gamma_i)\leqslant 0$, $y'>-a$

The integral G_1 may be rewritten as follows

$$G_1 = \frac{1}{\pi}\int_0^{\infty}\frac{j}{\gamma_1+\gamma_2}e^{j\gamma_1(y+a)}e^{-j\gamma_2(y'+a)}\cos\alpha\left(x-x'\right)d\alpha$$
$$+\frac{1}{2\pi}\int_{\alpha_0}^{\infty}\frac{1}{\alpha}e^{-\alpha(y'-y)}\cos\alpha\left(x-x'\right)d\alpha - \frac{1}{2\pi}\int_{\alpha_0}^{\infty}\frac{1}{\alpha}e^{-\alpha(y'-y)}\cos\alpha\left(x-x'\right)d\alpha$$

in general, we choose $\alpha_0 \gg |k_i|$,$i=1,2$

By Eq. (A1), we get

$$-\frac{1}{2\pi}\int_{\alpha_0}^{\infty}\frac{1}{\alpha}e^{-\alpha(y'-y)}\cos\alpha(x-x')d\alpha = -\frac{1}{4\pi}\{\Gamma[0,[(y-y')+j(x-x')]\alpha_0]$$
$$+\Gamma[0,[(y-y')-j(x-x')]\alpha_0]\}$$

Using the above relation, we obtain

$$G_1 = \frac{1}{\pi}\int_0^{\infty}\frac{j}{\gamma_1+\gamma_2}e^{j\gamma_1(y+a)}e^{-j\gamma_2(y'+a)}\cos\alpha\left(x-x'\right)d\alpha$$
$$+\frac{1}{2\pi}\int_{\alpha_0}^{\infty}\frac{1}{\alpha}e^{-\alpha(y'-y)}\cos\alpha\left(x-x'\right)d\alpha \tag{A3}$$
$$-\frac{1}{4\pi}\left\{\Gamma\left[0,\left[(y-y')+j(x-x')\right]\alpha_0\right]+\Gamma\left[0,\left[(y-y')-j(x-x')\right]\alpha_0\right]\right\}$$

Now, the integral G_1 is written as a rapidly converging integral plus a dominant integral which can be calculated by means of Simpson's rule easily.

Similarly, we can have

$$
\begin{aligned}
G_S &= \frac{1}{2\pi}\int_{-\infty}^{\infty}\frac{J}{2\gamma_2}\left(\frac{\gamma_1-\gamma_2}{\gamma_1+\gamma_2}\right)e^{-j\gamma_2(y+2a+y')}e^{-j\alpha(x-x')}d\alpha \\
&= \left[\frac{1}{\pi}\int_0^{\infty}\frac{j}{2\gamma_2}\left(\frac{\gamma_2-\gamma_1}{\gamma_2+\gamma_1}\right)e^{-j\gamma_2(y+2a+y')}\cos\alpha(x-x')d\alpha - \frac{k_2^2-k_1^2}{8\pi}\int_{\alpha_0}^{\infty}\right. \\
&\quad \left.\frac{1}{\alpha_0^3}e^{-\alpha(y+2a+y')}\cos\alpha(x-x')d\alpha\right] \\
&\quad + \frac{k_2^2-k_1^2}{16\pi}\left\{\begin{array}{l}\left[(y+2a+y')+j\,(x-x')\right]^2\Gamma\left[-2,\left[(y+2a+y')+j\,(x-x')\right]\alpha_0\right]+ \\ \left[(y+2a+y')-j\,(x-x')\right]^2\Gamma\left[-2,\left[(y+2a+y')-j\,(x-x')\right]\alpha_0\right]\end{array}\right\}
\end{aligned}
$$

References

[1] A. Roger, Newton-Kantorovitch algorithm applied to an electromagnetic inverse problem, *IEEE Trans. Antennas Propagat* **AP-29** (Mar. 1981), 232–238.

[2] C.C. Chiu and Y.W. Kiang, Inverse scattering of a buried conducting cylinder, *Inverse Problems* **7** (April, 1991), 187–202.

[3] C.C. Chiu and Y.W. Kiang, Microwave imaging of multiple conducting cylinders, *IEEE Trans. Antennas Propagat.* **40** (Aug. 1992), 933–941.

[4] G.P. Otto and W.C. Chew, Microwave inverse scattering-local shape function imaging for improved resolution of strong scatterers, *IEEE Trans. Microwave Theory Tech* **42** (Jan. 1994), 137–142.

[5] R. Kress, in: *A Newton method in inverse obstacle scattering Inverse Problem in Engineering Mechanics*, H.D. Bui, et al., (Rotterdam: Balkema), (1994), pp. 425–432.

[6] D. Colton and P. Monk, A novel method for solving the inverse scattering problem for time-harmonic acoustic waves in the resonance region II, *SIAM J. Appl. Math* **46** (June, 1986), 506–523.

[7] A. Kirsch, R. Kress, P. Monk and A. Zinn, Two methods for solving the inverse acoustic scattering problem, *Inverse problems* **4** (Aug. 1998), 749–770.

[8] F. Hettlich, Two methods for solving an inverse conductive scattering problem, *Inverse Problems* **10** (1994), 375–385.

[9] R.E. Kleinman and P.M. van den Berg, Two-dimensional location and shape reconstruction, *Radio Sci.* **29** (July-Aug. 1994), 1157–1169.

[10] T. Hohage, *Iterative methods in inverse obstacle scattering: regularization theory of linear and nonlinear exponentially ill-posed problems*, Dissertation Linz, 1999.

[11] D.E. Goldgreg, *Genetic Algorithm in Search*, Optimization and Machine Learning, Addison-Wesley, 1989.

[12] C.C. Chiu and P.T. Liu, Image reconstruction of a perfectly conducting cylinder by the genetic algorithm, *IEE Proc. Microw. Antennas Propag* **143** (June, 1996), 249–253.

[13] F. Xiao and H. Yabe, Microwave imaging of perfectly conducting cylinders from real data by micro genetic algorithm couple with deterministic method, *IEICE Trans. Electron* **E81-C** (Dec. 1998).

[14] Z.Q. Meng, T. Takenaka and T. Tanaka, Image reconstruction of two- dimensional impenetrable objects using genetic algorithm, *Journal of Electromagnetic Waves and Applications* **13** (1999), 95–118.

[15] Z. Qian, Z. Ding and W. Hong, *Application of genetic algorithm and boundary element method to electromagnetic imaging of two-dimensional conducting targets*, 5th International Symposium on ISAPE, 2000, pp. 211–214.

[16] C.L. Li, S.H. Chen, C.M. Yang and C.C. Chiu, Image reconstruction for a patially immersed perfectly conducting cylinder using the steady state algorithm, *Radio Science* **39** RS2016, April, 2004.

[17] F.M. Tesche, On the inclusion of loss in time domain solutions of electromagnetic interaction problems, *IEEE Trans. Electromagn. Compat.* **32** (1990), 1–4.

[18] E.C. Jordan and K.G. Balmain, *Electromagnetic Waves and Radiating systems. Englewood Cliffs*, NJ: Prentice-Hall, 1968.

[19] R.F. Harrington, *Field Computation by Moment Methods*, Macmillan: New York, 1968.